Carbohydrate Polymers 115 (2015) 686–693

Contents lists available at ScienceDirect

Carbohydrate Polymers

journal homepage: www.elsevier.com/locate/carbpol

Porous chitosan doped with graphene oxide as highly effective adsorbent for methyl orange and amido black 10B

Ying Wang [a], Guangmei Xia [b], Cong Wu [a], Jing Sun [c], Rui Song [a,*], Wei Huang [d]

[a] College of Chemistry and Chemical Engineering, University of Chinese Academy of Sciences, Beijing 100049, China
[b] Beijing National Laboratory for Molecular Sciences, CAS Key Laboratory of Engineering Plastics, Institute of Chemistry, Chinese Academy of Sciences, Beijing 100190, China
[c] Shanghai Institute of Microsystem and Information Technology, Chinese Academy of Sciences, Shanghai 200050, China
[d] Laboratory of Advanced Polymer Materials, Institute of Chemistry, Chinese Academy of Sciences, Beijing 100080, China

ARTICLE INFO

Article history:
Received 16 June 2014
Received in revised form 14 August 2014
Accepted 6 September 2014
Available online 23 September 2014

Keywords:
Chitosan
Graphene oxide
Methyl orange
Amido black 10B
Adsorption

ABSTRACT

In the current study, porous chitosan aerogels doped with small amount of graphene oxide (CSGO aerogels) with high porosity (97.96–98.78%), extraordinarily high water absorption (5848–8917%) and low density (0.021–0.035 g cm^{-3}) were prepared and used as adsorbents for two azo dyes methyl orange (MO) and amido black 10B (AB10B). The adsorption behavior of these CSGO aerogels and some influence factors such as pH value, graphene oxide (GO) loading, concentration of pollutants, as well as adsorption kinetics were studied. Specifically, the adsorption capacity for MO is 686.89 mg g^{-1}, the highest comparing with other publication results, and it is 573.47 mg g^{-1} for AB10B. Since they are biodegradable, non-toxic, efficient, low-cost and easy to prepare, we believe that these porous CSGO aerogels will be a promising candidate for dye removal.

1. Introduction

Nowadays the treatment of dyeing effluents has long been a major concern. Most dye molecules in the effluent are known to be toxic, mutagenic and carcinogenic (Chatterjee, Chatterjee, Lim, & Woo, 2011b). Azo dyes constitute the largest class of colorants and are common aquatic pollutants, which own the —N=N— chromophore group and the aromatic structure. They are normally difficult to remove because they are largely non-biodegradable and are resistant to light and oxidizing agents (Anirudhan, Radhakrishnan, & Vijayan, 2013; Cheah et al., 2013), and adsorption process is proven as a reliable and effective act for this dye treatment (Cheah et al., 2013; Vimonses, Lei, Jin, Chow, & Saint, 2009). Aerogel is a porous material and has been used in the area of organic pollutants adsorption. Rao, Hegde and Hirashima (2007) investigated the adsorption of organic liquids on silica aerogel and found that the aerogel could adsorb the organic liquids and oils by nearly 15 times of its own mass. Abramian and El-Rassy (2009) prepared titania aerogels by supercritical drying of wet alcogels which are synthesized through a one-pot sol–gel process and its adsorption capacity for Orange II is 420 mg g^{-1} at the optimal conditions.

Chitosan (CS), the cationic (1-4)-2-amino-2-deoxy-β-D-glucan, is mainly produced from marine chitin by deacetylation (Muzzarelli et al., 2012). As one of the most representative biopolymers, it is a multifunctional polysaccharide comprising of copious chelating groups including primary and secondary hydroxyl groups, as well as highly reactive amino groups (Rinaudo, 2006). Meanwhile, it is low-cost, non-toxic and biodegradable, so it has been considered as a green adsorbent for the removal of dyes (Crini & Badot, 2008; Chatterjee, Chatterjee, Lim, & Woo, 2011a). However, the application of chitosan is limited because of its solubility in acid solution. Hence, it is necessary to crosslink chitosan in order to make it stable in acid solution (Liu et al., 2012).

Graphene oxide (GO) is an oxygen-rich carbonaceous layered material. It has gained considerable attention as a significant adsorbent as plenty of oxygen atoms on the basal plane and the edge of the sheets in the forms of epoxy, hydroxyl, and carboxyl groups, protruding from its layers (Chen, Chen, Bai, & Li, 2013; Travlou, Kyzas, Lazaridis, & Deliyanni, 2013). Meanwhile, as a significant carbonaceous layered material, the GO incorporation can enhance the strength of polymer composites (Zhang, Qiu, Si, Wang, & Gao, 2011). Therefore, it will be interesting to prepare porous CS materials with incorporation of GO.

* Corresponding author. Tel.: +86 10 8825 6843; fax: +86 10 8825 6092.
E-mail address: rsong@gucas.ac.cn (R. Song).

http://dx.doi.org/10.1016/j.carbpol.2014.09.041
0144-8617/

In this work, we prepared porous chitosan aerogels doped with graphene oxide (CSGO aerogels) by crosslinking and freeze drying and used them as highly effective adsorbents for two azo dyes, methyl orange (MO) and amido black 10B (AB10B), which are widely used in chemical, textile, paper industries, biological stain, paints, inks, plastics, and leather industries (Jalil et al., 2010; Mittal, Thakur, & Gajbe, 2013). Its adsorption capacity for MO is 686.89 mg g^{-1}, which is the highest compared to those existing literatures, and the adsorption capacity for AB10B also reaches 573.47 mg g^{-1}. Meanwhile, the effects of pH values, concentration of pollutants, loading of graphene oxide on the adsorption for MO and AB10B as well as adsorption kinetics were studied.

2. Experiment

2.1. Materials

CS (Mn = 700 K, degree of deacetylation (DD) = 95%) was purchased from Zhejiang Yuhuan Marine Bio-chemical Co. Ltd. GO was prepared by Hummer's method, and the detail about its synthesis could be found elsewhere (Cao, Yin, & Song, 2013). Acetic acid, nitric acid, sodium hydroxide were analytical-grade while MO and AB10B were biological stain and they were all from commercial suppliers (Sinopharm, Beijing) and used without further purification. Methyl aldehyde (37% w/w aqueous solution) was from Alfa Aesar.

2.2. Preparation of porous CSGO aerogels

Firstly, various amounts of GO aqueous solution (8 mg mL^{-1}) were added to 2% (V/V) acetic acid aqueous solution to form GO acetic acid aqueous solution (solution A). Then 0.6 g CS was dissolved into 15 ml solution A and formed homogeneous CSGO mixture after being stirred for 1 h. Subsequently, 20 μL 37% methyl aldehyde aqueous solution was added to the CSGO mixture dropwise with stirring in water bath at 50 °C and then CSGO hydrogels were formed in 1 min, following 1 h standstill at 50 °C. After that we cut these hydrogels into small pieces and put them into water to swell for 40 min. Subsequently, the swollen hydrogels were frozen below −18 °C and then transferred to a lyophilizer (FD-1CE, Boyikang Co. Ltd., Beijing) with a condenser temperature of −55 °C and inside pressure 20–30 Pa. After 2-day lyophilization process CSGO aerogels were obtained.

In this case, CSGO aerogels with different GO contents, which is 1 wt% (CSGO1), 3 wt% (CSGO3), were prepared, respectively. Similarly, CS aerogel was prepared in the absence of GO.

2.3. Calculation of the water absorption of CSGO aerogels

These CSGO aerogels were put into deionized water for 1 h, and their water adsorption was calculated according to the following equation:

$$\text{Water absorption } (\%) = \frac{(M_t - M_0)}{M_0} \times 100\%$$

where M_0 (g) and M_t (g) are the weight of the CSGO aerogels before and after immersing into deionized water, respectively.

2.4. Porosity and density of porous CSGO aerogels

The porosity and apparent density of the porous CSGO aerogels was calculated according to the following equation:

$$\text{Porosity } (\%) = \frac{(V_t - V_a)}{V_t} \times 100\% = \frac{\left(V_t - M_a/\rho\right)}{V_t} \times 100\%$$

$$\text{Density} = \frac{V_t}{M_a}$$

where V_t (cm^3) is the total volume of CSGO aerogels, V_a (cm^3) is the actual volume of the material, M_a (g) is the mass of the aerogels, and ρ (g cm^{-3}) is the actual density of the material. Each sample was measured in triplicate and the average value was adopted.

2.5. Batch adsorption experiments

The stored MO and AB10B solution were prepared by directly dissolving these compounds with known weight in deionized water. Batch adsorption experiments were carried out in 25 mL flasks, where M = 0.013–0.015 g of the adsorbents were put into V = 13–15 mL of MO or AB10B aqueous solutions (the V/M was kept at 1 L g^{-1}) and allowed to adsorb at room temperature (20 ± 1 °C) without stirring or shaking. At given time intervals, the concentrations of pollutant solutions were measured and adsorbents were collected. The dye concentration was determined by the absorbance at 464 nm for MO and 610 nm for AB10B in the ultraviolet–visible (UV–vis) spectrum.

The adsorption capacity (Q) and adsorption efficiency (Ade) was calculated according to the following equation:

$$Q_t = \frac{(C_0 - C_t)}{M} V$$

$$\text{Ade } (\%) = \frac{(C_0 - C_t)}{C_0} \times 100\%$$

where C_0 (mg L^{-1}) and C_t (mg L^{-1}) are the concentrations of pollutants in solution after 0 and t h, V (L) is the volume of solution and M (g) is the mass of the adsorbent. Q_t (mg g^{-1}) is the apparent adsorption capacity of the porous monoliths after t h, which if given a long enough adsorption period (the time required to achieve the equilibrium adsorption state), is equal to the equilibrium adsorption capacity Q_e (mg g^{-1}).

The time required to achieve the equilibrium adsorption state (t_e) was determined by the adsorption kinetic curve. The adsorption time in the adsorption experiments measuring Q_e was set longer than t_e.

2.6. Characterization

X-ray powder diffraction data were collected on MSAL-XD3 with Cu $K\alpha$ radiation (λ = 0.1542 nm) at 40 kV and 40 mA. Scanning electron microscopy was performed on a field emission SEM (Hitachi S-4800) at an accelerating voltage of 10 kV. Thermo gravimetric analyzer curves were determined by SDT-Q600 analyzer (TA Corp., US) at a heating rate of 10 °C min^{-1} in N_2 atmosphere. UV-visible spectra were recorded on a UV-2550 (Shimadzu Corporation, Japan) at room temperature.

Fourier transform infrared spectroscopy was carried out on a Nicolet VERTEX 70 (Bruker) spectrometer using the attenuated total reflectance (ATR) method at a resolution of 4 cm^{-1}. The spectrum was generated and collected 16 times and corrected for the background noise.

X-ray photoelectron spectrometer (XPS) measurements were taken via an ESCALAB250Xi (Thermo Scientific, USA) using a unmonochromatic Al $K\alpha$ line at 1486.6 eV in an ultra-high-vacuum system with a base pressure 3×10^{-9} mbar and an analyzer pass energy of 150 eV, giving a full width at half-maximum of 1.7 eV for the Au $4f_{7/2}$ peak. The binding-energy scale was calibrated by assigning the main C1s peak at 284.8 eV. The XPS core-level spectra were analyzed by decomposing each spectrum into individual mixed Gaussian–Lorentzian peaks.

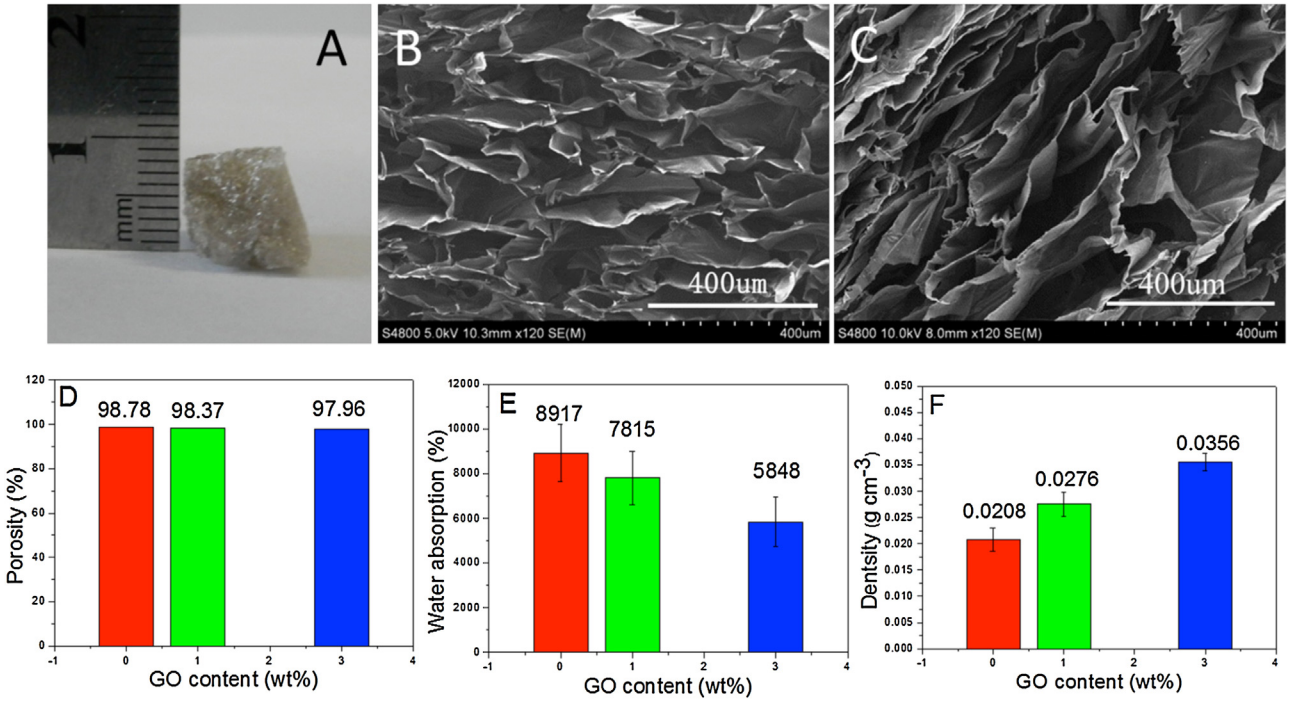

Fig. 1. Optical image (A) of CSGO1 aerogel; SEM image of CSGO1 (B) and CSGO3 (C) aerogels. Porosity (D), water absorption (E) and density (F) of the prepared CSGO aerogels with different GO contents.

Dynamic mechanical properties were measured using a dynamic mechanical analyzer (DMA Q800, TA, US). Tests were carried out in the DMA multi-frequency–strain module with frequency of 0.1–15 Hz at a 35°C. Compressive strength of the porous CSGO aerogels were measured by material testing machine (HY-0580, Hengyi Corp., Shanghai) with 50% compressed at a compressing rate of 2 mm min^{-1}. The samples for compressive strength were prepared without swelling in water for 40 min before freeze drying. Each sample was measured in triplicate and the average value was adopted.

3. Results and discussion

3.1. Characterization of the CSGO aerogels

Fig. 1A–C shows the optical and SEM images of the CSGO aerogels, indicating the porous network structure of the prepared aerogels. Fig. 1D–F reveals water absorption, porosity and density of the prepared CSGO aerogels. All the obtained aerogels have high porosity (97.96–98.78%), extraordinarily high water absorption ability (5848–8917%) and low density (0.021–0.035 g cm^{-3}). The high porosity and water absorption ability should contribute to the diffusion of dyes to the surface and interior regions of the porous CSGO aerogels, leading to high adsorption abilities and rates for dyes.

Fig. 2 shows the XRD spectra of GO, CS and CSGO aerogels. Both the CS and CSGO aerogels show a characteristic peak at about $2\theta = 12.34°$ and 20.25° attributed to chitosan, and no distinct changes are observed with the increase of GO content, indicating that the GO has no obvious influence on the crystalline properties of CS (Zhang et al., 2011). Meanwhile, the characteristic diffraction peak of GO at $2\theta = 11.76°$ is not clearly demonstrated in the CSGO aerogels because of its low content.

Fig. 3A shows the FTIR spectra of CS, CSGO aerogels and GO. Spectrum of GO shows characteristic absorption bands of vibration of C—O at 1042 cm^{-1}, C=C stretching mode of the sp^2 carbon skeletal network at 1620 cm^{-1} and the stretching vibration of carboxyl groups on the edges of the layer planes or conjugated carbonyl groups at about 1714 cm^{-1}, respectively (Szabó et al., 2006; Titelman et al., 2005; Seredych, Petit, Tamashausky, & Bandosz, 2009; Travlou et al., 2013). In comparison, all the GO-related peaks are not detected in the CSGO spectra because of GO's low content. The band at 1551 cm^{-1} corresponds to N—H bending of $-NH_2$ (Fan et al., 2012; Ma, Liu, Li, & Wang, 2012a). In the case of GO doped by 1% to 3%, the band of $-NH_2$ has shifted to a lower value from 1551 cm^{-1} to 1540 cm^{-1}, which proves that $-NH_2$ groups on the CS chains have been reacted with the oxygen-containing functional groups of GO (Fan et al., 2012).

To further confirm the above issue, X-ray photoelectron spectra of CS, CSGO1 and CSGO3 aerogels were analyzed (Fig. 3B and C). The O1s spectra were curve-fitted by two peaks: the first peak at 532.1 eV is due to O—H groups, and the second at about 532.7 eV is relevant to O—C moieties (epoxy, carboxyl groups) (Travlou et al., 2013). The peak attributed to O—H groups increased in these CSGO aerogels, indicating the O—H formation by the reaction of the chitosan amino groups with the oxygen-containing functional group of GO, which is consistent with the FTIR result. The reaction mechanism can be shown as follow:

$$R_1\text{-}NH_2 + : O\text{-}R_2 \rightarrow R_1\text{-}NH_2 \cdots O\text{-}R_2$$

where R_1 is the remaining structure besides $-NH_2$ of chitosan, R_2 is the remaining structure besides –O: of GO.

The mechanical properties of the CSGO aerogels were investigated by the compression tests and the dynamic mechanical analysis (DMA), as shown in Fig. 4A–C. The compressive strength of the obtained samples was increased with the increase of GO content (Fig. 4A). The viscoelastic property and inter-structure can be further assessed by DMA test. For both CS and CSGO1 aerogels, the storage modulus value is much higher than the loss modulus value over the entire angular frequency (0.1–15 rad s^{-1}), which reveals that the elastic response is predominant, implying that these aerogels have a permanent network (Wu et al., 2013). The

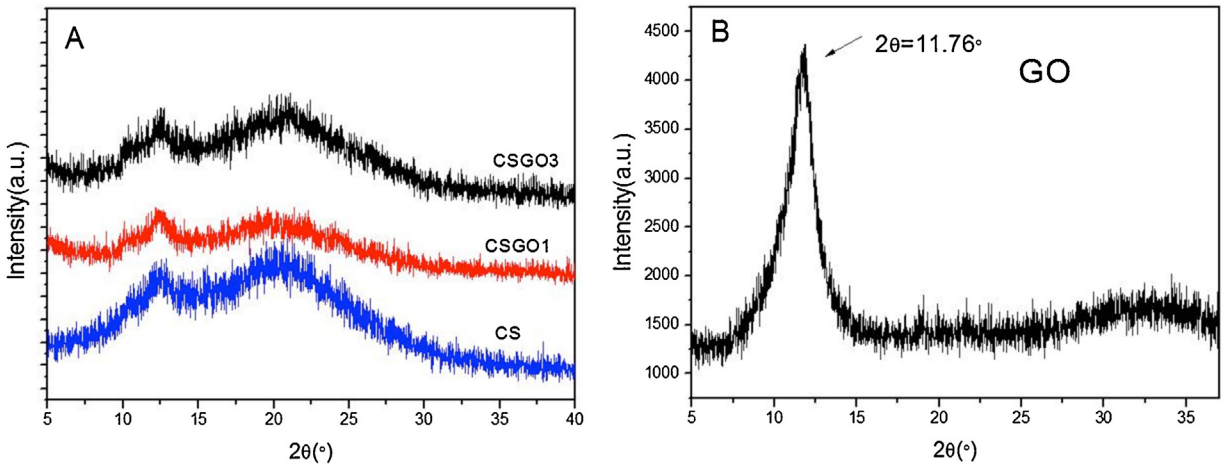

Fig. 2. XRD spectra of CS and CSGO aerogels (A) and GO (B).

storage modulus increases from 2.2–3.1 MPa to 3.3–4 MPa with the addition of 1 wt% GO, while the loss modulus decrease from 0.31–0.66 MPa to 0.1–0.4 MPa, indicating that GO can improve the elastic response of the prepared aerogel.

Thermogravimetric (TG) analysis was carried out to investigate thermal decomposition behavior of the CSGO aerogels, as shown in Fig. 4E and F. The differential thermogravimetric (DTG) curve of CSGO presents two peaks with maxima at 180 °C and 280 °C, respectively, corresponding to the two weight loss stage of the thermogravimetry curves. The first peak is related to the decomposition of surface functional groups of GO and the second peak related to the degradation of chitosan based on the previous reports (Travlou et al., 2013) and current results of pure GO and CS. The CSGO aerogels show almost identical thermogravimetric curves regardless of the different GO contents, indicating that low content of GO has no detectable effect on the thermal stability of the CSGO material.

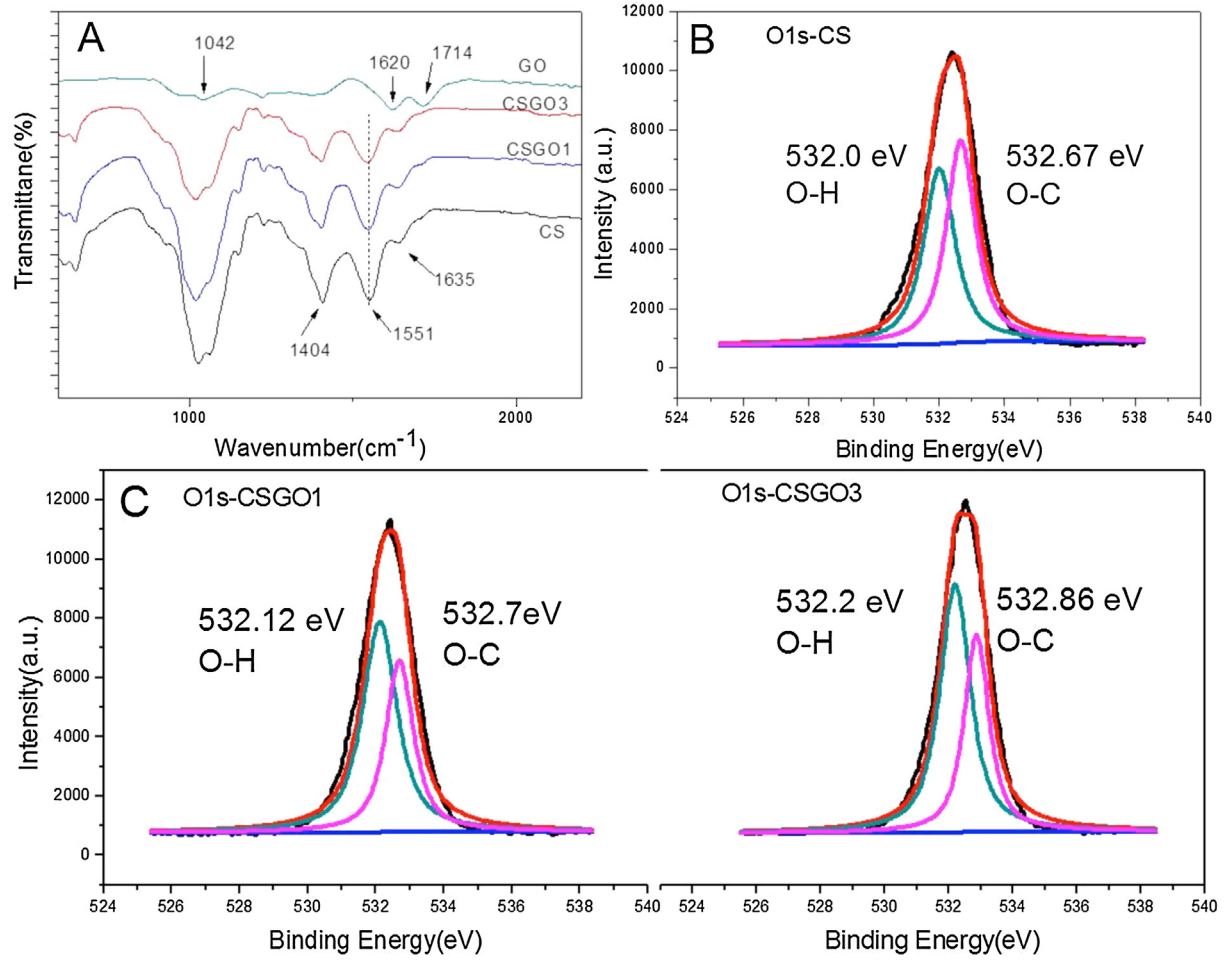

Fig. 3. FTIR spectra of CS, GO, CSGO1 and CSGO3 aerogels (A); O1s XPS spectra of neat CS (B) and CSGO1, CSGO3 aerogels (C).

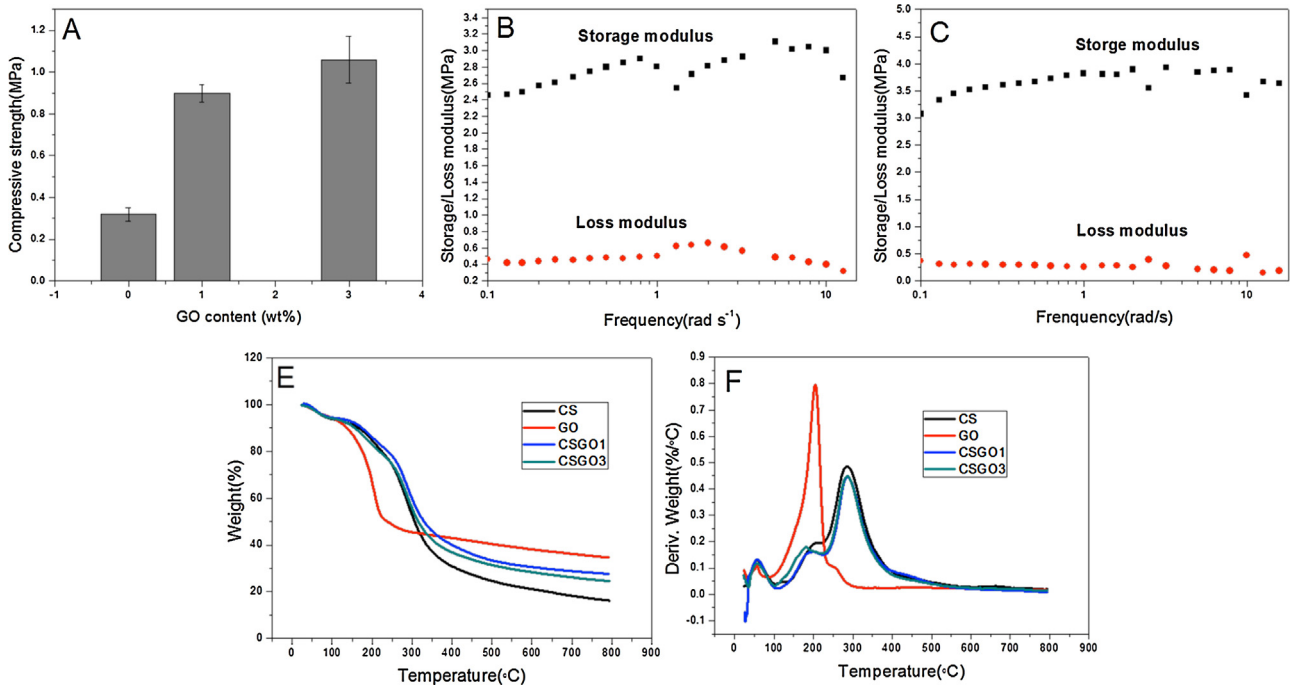

Fig. 4. Histograms of the compressive strength of CS, CSGO1 and CSGO3 aerogels (A). Dynamic mechanical analysis of CS aerogel (B) and CSGO1 aerogel (C). Thermogravimetry (E) and differential thermogravimetry (F) curves of GO, CS, CSGO1 and CSGO3.

3.2. Adsorption of MO and AB10B by CSGO aerogel

3.2.1. Effect of pH

Fig. 5A and B shows the equilibrium adsorption capacity for MO and AB10B of the CSGO1 aerogel in 800 mg L^{-1} initial dye solution with different pH values, which were adjust at first and allowed to be free during adsorption. For both MO and AB10B, the adsorption ability of the CSGO1 aerogel decreases with the increasing of pH values. It is because the main force of the adsorption is electrostatic attraction between the MO/AB10B and the protonated amino groups. At lower pH, the amino groups of the CS macromolecules become protonated, and electrostatic attraction between the MO/AB10B and the protonated amino groups may contribute to the adsorption of the MO/AB10B onto the CSGO aerogel (Travlou et al., 2013).

3.2.2. Effect of GO content

Fig. 5C and D shows the equilibrium adsorption capacity for MO and AB10B of the prepared aerogels in 800 mg L^{-1} initial dye solution at pH 8.45 and 7.79, respectively. The result show that the addition of 1 wt% or 3 wt% GO has almost no effect on the adsorption capacity. The reason can be attributed two aspects. On one hand, recent reports shows that GO exhibits low affinity for anionic dyes, due to the strong electrostatic repulsion between them (Chen et al., 2013; Travlou et al., 2013). On the other hand, although GO may enhance adsorption ability for dyes when introduced into the porous material, the existence of carboxyl groups might reduce the binding capacity of the amine groups for dyes due to electrostatic forces between the carboxyl and amine groups, which may decrease the adsorption capacity of the CSGO aerogel (Zhang et al., 2011). These two aspects cause the limited growth of the adsorption capacity as a whole.

3.2.3. Effect of contact time (adsorption kinetics)

Fig. 5E and F shows the effect of contact time on dye adsorption of CSGO1 aerogel in 800 mg L^{-1} MO and AB10B solution. For the MO adsorption, very fast dye removal occurs at the initial stage (0–10 h). Then, the dye adsorption is milder and more gradual during the second time period (10–60 h). And at the last stage (60–84 h) the dye adsorption is characterized by the equilibrium state. The fast adsorption in the initial stage might be due to the fact that a large number of surface sites are available for adsorption. After a period of adsorption, the remaining surface sites are more resistive for the dye molecules to occupy because of the repulsion between the solute molecules of the solid and bulk phases, which makes it milder and take a long time to reach equilibrium (Travlou et al., 2013). And AB10B displays the similar adsorption behavior.

To investigate the controlling mechanism of the adsorption processes, pseudo-first-order and pseudo-second-order kinetic models were used to study the experimental data obtained.

The pseudo-first-order kinetic model is given as (Chiou, & Li, 2002; Jiang, Fu, Zhu, Yao, & Xiao, 2012)

$$\log(Q_e - Q_t) = \log Q_e - \frac{K_1}{2.303}t$$

The pseudo-second-order kinetic model can be expressed as (Chiou & Li, 2002; Jiang et al., 2012)

$$\frac{t}{Q_t} = \frac{1}{k_2 Q_e^2} + \frac{t}{Q_e}$$

where Q_e and Q_t are the amounts of MO/AB10B adsorbed (mg g^{-1}) per unit of adsorbent at equilibrium and at time t, respectively. k_1 is the pseudo-first-order rate constant (h^{-1}). The rate constant (k_1) and correlation coefficients (R^2) are determined from the linear plots of $\log(Q_e - Q_t)$ *versus* t. k_2 is the pseudo-second-order rate constant of adsorption (g mg^{-1} h^{-1}). The rate constant (k_2) and correlation coefficients (R^2) are determined from the linear plots of t/Q_t *versus* t.

According to the correlation coefficients (R^2), the pseudo-second-order equation provided an excellent fit for the experimental data of both MO ($R^2 = 0.9995$) and AB10B ($R^2 = 0.9988$)

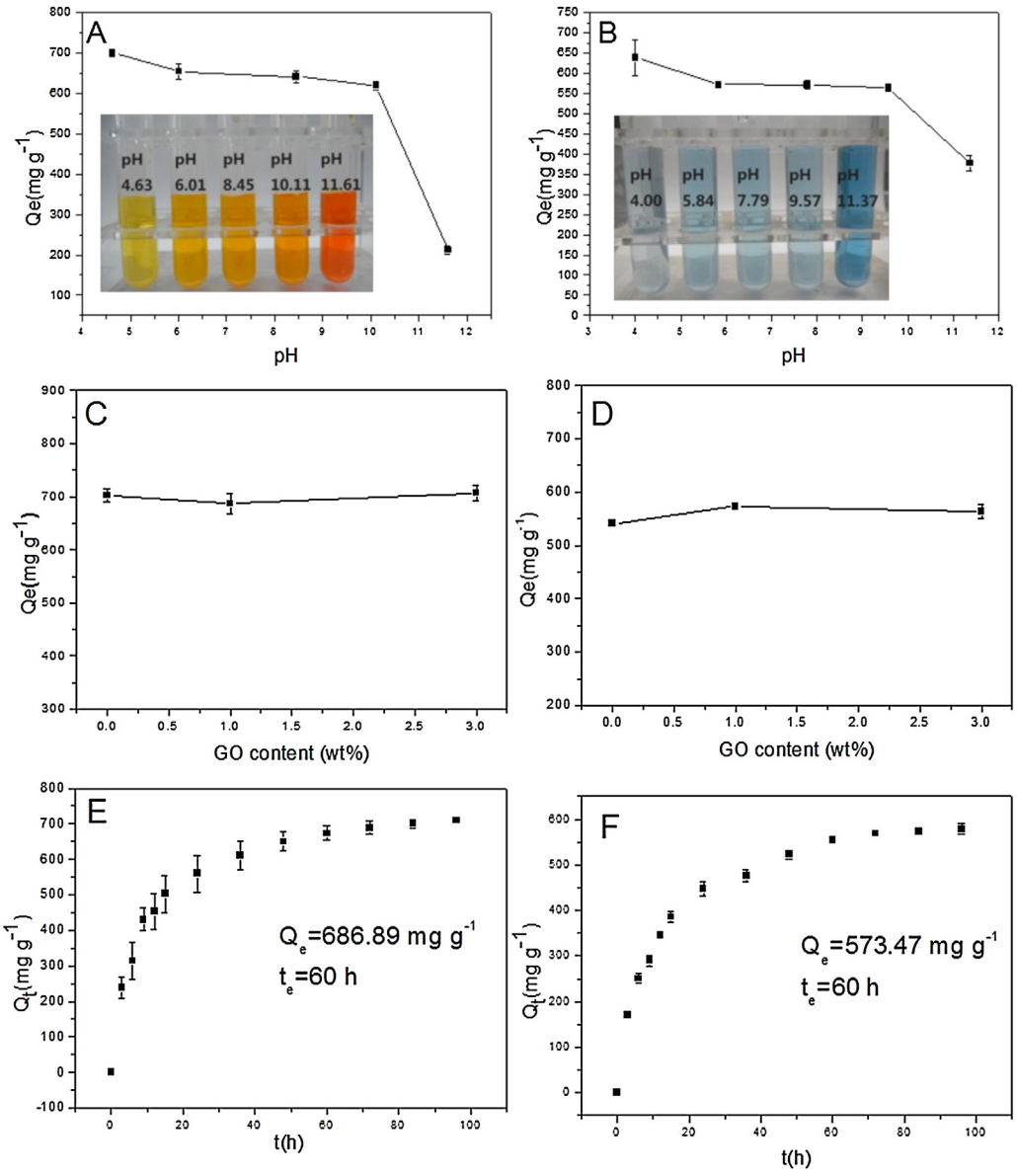

Fig. 5. Adsorption of the CSGO1 aerogel for MO ((A), (C), (E)) and AB10B ((B), (D), (F)) in solutions (800 mg L^{-1}) with different pH values, GO contents and time, respectively. Inset: optical images of diluted dye solution after adsorption.

adsorption, compared with the (R^2) data from pseudo-first-order equation, 0.9814 for MO and 0.9405 for AB10B, respectively.

3.2.4. Adsorption mechanism

We discuss the adsorption mechanism by FTIR (Fig. 6) and take the adsorption for AB10B as a representative. As shown, the amino peak at 1546 cm^{-1} of CSGO1 aerogel after dye adsorption presents a decrease and shifts to a lower wavenumber, which confirms the mechanism explaining the interactions between the dye molecules and adsorbents (Travlou et al., 2013; Liu, Zheng, & Wang, 2010).

The resultant CSGO1 aerogel presents a prominent adsorption capacity for MO and AB10B comparing with other reported adsorbents, and detail could be found in Tables 1 and 2. As indicated, the adsorption capacity (Q) of the prepared porous CSGO1 aerogel is much higher than most reported adsorbents. In particular, the CSGO1 aerogel owns the highest Q value of MO among the related publications available. So the prepared porous CSGO aerogels can be a kind of promising adsorbent for the removal of MO and AB10B

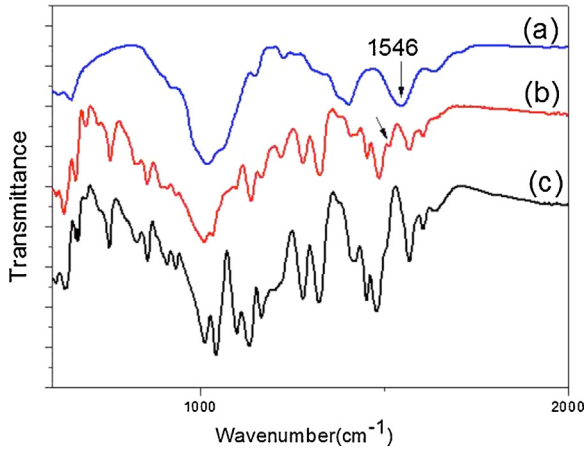

Fig. 6. FTIR spectra of CSGO1 aerogel (a), AB10B loaded CSGO1 aerogels (b) and AB10B dye (c).

Table 1
Comparison of the adsorption capacity of CSGO1 aerogel for MO removal with other adsorbents.

Adsorbents	$Q\,(mg\,g^{-1})$
γ-Fe_2O_3/chitosan composite films (Jiang et al., 2012)	29.41
γ-Fe_2O_3/MWCNTs/chitosan (Zhu, Jiang, Xiao, & Zeng, 2010)	60.5–66.1
Hypercrosslinked chloromethylated PS adsorbent functionalized with formaldehyde carbonyl groups (HJ-1) (Huang, Huang, Liu, Wang, & Yan, 2008)	70.9–76.9
mesoporous magnetic Co-NPs/carbon nanocomposites (Zhang, An, Guo, & Wang, 2013)	380
Acid modified carbon coated monolith (Cheah et al., 2013)	132.7
Calcined layered double hydroxides (Ni, Xia, Wang, Xing, & Pan, 2007)	200
Alkali-Activated Multiwalled Carbon Nanotubes (Ma et al., 2012b)	149
Pinecone derived activated carbon (Samarghandi, Hadi, Moayedi, & Askari, 2009)	404.4
Carbon nanotubes (Yao, Bing, Feifei, & Xiaofeng, 2011)	35.4–64.7
Chitin/alginate magnetic nano-gel beads (MCAs) (Li, Du, Tao, Deng, Luo, & Yang, 2010)	107.5
Porous CSGO1 aerogel (this work)	686.89

Table 2
Comparison of the adsorption capacity of CSGO1 aerogel for AB10B removal with other adsorbents.

Adsorbents	$Q\,(mg\,g^{-1})$
protonated crosslinked chitosan (Huang, Yang, Liu, & Gong, 2013)	9.43
Cross-linked chitosan (Yang, Huang, & Liu, 2012)	11.47
cross-linked amino-starches (Cheng, Jiang, Ou, Li, & Xiang, 2009)	990.10
Activated carbon prepared from scrap tires (Hoseinzadeh, Rahmanie, Asgari, McKay, & Dehghanian, 2012)	14.51
Conducting polyaniline/iron oxide composite (Ahmad, & Kumar, 2010)	About 60
Porous CSGO1 aerogel (this work)	573.47

from aqueous solutions owing to its very high adsorption capacity, low-cost, eco-friendly and easy preparation.

4. Conclusions

We have prepared porous chitosan aerogels doped with graphene oxide (CSGO aerogels) as highly effective adsorbent for two azo dyes MO and AB10B. These aerogels have the property of high porosity (97.96–98.78%), extraordinarily high water absorption (5848–8917%) and low density (0.021–0.035 $g\,cm^{-3}$). Its adsorption capacity for methyl orange (MO) can reach 686.89 $mg\,g^{-1}$, which is the highest compared to those existing literature, and the adsorption capacity for AB10B is 573.47 $mg\,g^{-1}$. Characterization of CSGO aerogels shows that $-NH_2$ groups on the CS chains have been reacted with the oxygen-containing functional groups of GO, and the addition of GO can improve the compressive strength and elastic response of these aerogels; while low loading of GO present no obvious influence on the crystalline properties of CS and the thermal stability of the CSGO material.

Study of adsorption behavior shows that the adsorption ability of the CSGO aerogel decreases with the increasing of pH values, and the adsorption processes fit well with pseudo-second-order process. Since the prepared porous aerogels are biodegradable, non-toxic, efficient, low-cost and easy to prepare, these porous CSGO aerogels would be a potential alternative for dye removal, and the current investigations may pave a way to the facile fabrication of efficient CS-based porous materials for water purification and environment remediation.

Acknowledgments

This work was supported by the National Science Foundation of China (21072221, (21172252). Supports from Mrs. Jin Huang, Institute of Organic Chemistry, CAS (Shanghai, China) for DMA test are also appreciated.

References

Abramian, L., & El-Rassy, H. (2009). Adsorption kinetics and thermodynamics of azo-dye Orange II onto highly porous titania aerogel. *Chemical Engineering Journal*, *150*(2–3), 403–410.
Ahmad, R., & Kumar, R. (2010). Conducting polyaniline/iron oxide composite: A novel adsorbent for the removal of amido black 10B. *Journal of Chemical & Engineering Data*, *55*(9), 3489–3493.
Anirudhan, T. S., Radhakrishnan, P. G., & Vijayan, K. (2013). Development of a first-order kinetics based model, equilibrium studies, and thermodynamics for the adsorption of methyl orange onto a lignocellulosic anion exchanger. *Separation Science and Technology*, *48*(6), 947–959.
Cao, J., Yin, H.-J., & Song, R. (2013). Circular dichroism of graphene oxide: The chiral structure model. *Frontiers of Materials Science*, *7*(1), 83–90.
Chatterjee, S., Chatterjee, T., Lim, S. R., & Woo, S. H. (2011a). Adsorption of a cationic dye, methylene blue, on to chitosan hydrogel beads generated by anionic surfactant gelation. *Environmental Technology*, *32*(13), 1503–1514.
Chatterjee, S., Chatterjee, T., Lim, S. R., & Woo, S. H. (2011b). Effect of the addition mode of carbon nanotubes for the production of chitosan hydrogel core–shell beads on adsorption of Congo red from aqueous solution. *Bioresource Technology*, *102*(6), 4402–4409.
Cheah, W., Hosseini, S., Khan, M. A., Chuah, T. G., & Choong, T. S. Y. (2013). Acid modified carbon coated monolith for methyl orange adsorption. *Chemical Engineering Journal*, *215–216*, 747–754.
Chen, Y., Chen, L., Bai, H., & Li, L. (2013). Graphene oxide–chitosan composite hydrogels as broad-spectrum adsorbents for water purification. *Journal of Materials Chemistry A*, *1*(6), 1992–2001.
Cheng, R., Jiang, Z., Ou, S., Li, Y., & Xiang, B. (2009). Investigation of acid black 1 adsorption onto amino-polysaccharides. *Polymer Bulletin*, *62*(1), 69–77.
Chiou, M.-S., & Li, H.-Y. (2002). Equilibrium and kinetic modeling of adsorption of reactive dye on cross-linked chitosan beads. *Journal of Hazardous Materials*, *93*(2), 233–248.
Crini, G., & Badot, P.-M. (2008). Application of chitosan, a natural aminopolysaccharide, for dye removal from aqueous solutions by adsorption processes using batch studies: A review of recent literature. *Progress in Polymer Science*, *33*(4), 399–447.
Fan, L., Luo, C., Li, X., Lu, F., Qiu, H., & Sun, M. (2012). Fabrication of novel magnetic chitosan grafted with graphene oxide to enhance adsorption properties for methyl blue. *Journal of Hazardous Materials*, *215–216*, 272–279.
Hoseinzadeh, E., Rahmanie, A. R., Asgari, G., McKay, G., & Dehghanian, A. R. (2012). Adsorption of acid black 1 by using activated carbon prepared from scrap tires: Kinetic and equilibrium studies. *Journal of Scientific & Industrial Research*, *71*(10), 682–689.
Huang, J.-H., Huang, K.-L., Liu, S.-Q., Wang, A. T., & Yan, C. (2008). Adsorption of Rhodamine B and methyl orange on a hypercrosslinked polymeric adsorbent in aqueous solution. *Colloids and Surfaces, A: Physicochemical and Engineering Aspects*, *330*(1), 55–61.
Huang, R., Yang, B., Liu, Q., & Gong, N. (2013). Adsorption of a model anionic dye on protonated crosslinked chitosan. *Desalination and Water Treatment*, 1–8. http://dx.doi.org/10.1080/19443994.2013.833139
Jalil, A. A., Triwahyono, S., Adam, S. H., Rahim, N. D., Aziz, M. A., Hairom, N. H., et al. (2010). Adsorption of methyl orange from aqueous solution onto calcined Lapindo volcanic mud. *Journal of Hazardous Materials*, *181*(1-3), 755–762.
Jiang, R., Fu, Y.-Q., Zhu, H.-Y., Yao, J., & Xiao, L. (2012). Removal of methyl orange from aqueous solutions by magnetic maghemite/chitosan nanocomposite films: Adsorption kinetics and equilibrium. *Journal of Applied Polymer Science*, *125*(S2), E540–E549.
Li, G., Du, Y., Tao, Y., Deng, H., Luo, X., & Yang, J. (2010). Iron(II) cross-linked chitin-based gel beads: Preparation, magnetic property and adsorption of methyl orange. *Carbohydrate Polymers*, *82*(3), 706–713.
Liu, L., Li, C., Bao, C., Jia, Q., Xiao, P., Liu, X., et al. (2012). Preparation and characterization of chitosan/graphene oxide composites for the adsorption of Au(III) and Pd(II). *Talanta*, *93*, 350–357.
Liu, Y., Zheng, Y., & Wang, A. (2010). Enhanced adsorption of methylene blue from aqueous solution by chitosan-g-poly(acrylic acid)/vermiculite hydrogel composites. *Journal of Environmental Sciences*, *22*(4), 486–493.
Ma, J., Liu, C., Li, R., & Wang, J. (2012). Properties and structural characterization of chitosan/graphene oxide biocomposites. *Bio-Medical Materials and Engineering*, *22*(1), 129–135.
Ma, J., Yu, F., Zhou, L., Jin, L., Yang, M., Luan, J., et al. (2012). Enhanced adsorptive removal of methyl orange and methylene blue from aqueous solution by alkali-activated multiwalled carbon nanotubes. *ACS Applied Materials & Interfaces*, *4*(11), 5749–5760.
Mittal, A., Thakur, V., & Gajbe, V. (2013). Adsorptive removal of toxic azo dye Amido Black 10B by hen feather. *Environmental Science and Pollution Research*, *20*(1), 260–269.

Muzzarelli, R. A. A., Boudrant, J., Meyer, D., Manno, N., DeMarchis, M., & Paoletti, M. G. (2012). Current views on fungal chitin/chitosan, human chitinases, food preservation, glucans, pectins and inulin: A tribute to Henri Braconnot, precursor of the carbohydrate polymers science, on the chitin bicentennial. *Carbohydrate Polymers*, *87*(2), 995–1012.

Ni, Z. M., Xia, S. J., Wang, L. G., Xing, F. F., & Pan, G. X. (2007). Treatment of methyl orange by calcined layered double hydroxides in aqueous solution: Adsorption property and kinetic studies. *Journal of Colloid and Interface Science*, *316*(2), 284–291.

Rinaudo, M. (2006). Chitin and chitosan: Properties and applications. *Progress in Polymer Science*, *31*(7), 603–632.

Samarghandi, M. R., Hadi, M., Moayedi, S., & Askari, F. B. (2009). Two-parameter isotherms of methyl orange sorption by pinecone derived activated carbon. *Iranian Journal of Environmental Health Science & Engineering*, *6*(4), 285–294.

Seredych, M., Petit, C., Tamashausky, A. V., & Bandosz, T. J. (2009). Role of graphite precursor in the performance of graphite oxides as ammonia adsorbents. *Carbon*, *47*(2), 445–456.

Szabó, T., Berkesi, O., Forgó, P., Josepovits, K., Sanakis, Y., Petridis, D., et al. (2006). Evolution of surface functional groups in a series of progressively oxidized graphite oxides. *Chemistry of Materials*, *18*(11), 2740–2749.

Titelman, G. I., Gelman, V., Bron, S., Khalfin, R. L., Cohen, Y., & Bianco-Peled, H. (2005). Characteristics and microstructure of aqueous colloidal dispersions of graphite oxide. *Carbon*, *43*(3), 641–649.

Travlou, N. A., Kyzas, G. Z., Lazaridis, N. K., & Deliyanni, E. A. (2013). Functionalization of graphite oxide with magnetic chitosan for the preparation of a nanocomposite dye adsorbent. *Langmuir*, *29*(5), 1657–1668.

Rao, Venkateswara A., Hegde, N. D., & Hirashima, H. (2007). Absorption and desorption of organic liquids in elastic superhydrophobic silica aerogels. *Journal of Colloid and Interface Science*, *305*(1), 124–132.

Vimonses, V., Lei, S., Jin, B., Chow, C. W. K., & Saint, C. (2009). Adsorption of congo red by three Australian kaolins. *Applied Clay Science*, *43*(3–4), 465–472.

Wu, X.-L., Wen, T., Guo, H.-L., Yang, S., Wang, X., & Xu, A.-W. (2013). Biomass-derived sponge-like carbonaceous hydrogels and aerogels for supercapacitors. *ACS Nano*, *7*(4), 3589–3597.

Yang, B., Huang, R., & Liu, Q. (2012). Adsorption of Amido black 10B onto cross-linked chitosan. *Research Journal of Chemistry and Environment*, *16*(3), 110–115.

Yao, Y., Bing, H., Feifei, X., & Xiaofeng, C. (2011). Equilibrium and kinetic studies of methyl orange adsorption on multiwalled carbon nanotubes. *Chemical Engineering Journal*, *170*(1), 82–89.

Zhang, N., Qiu, H., Si, Y., Wang, W., & Gao, J. (2011). Fabrication of highly porous biodegradable monoliths strengthened by graphene oxide and their adsorption of metal ions. *Carbon*, *49*(3), 827–837.

Zhang, P., An, Q., Guo, J., & Wang, C. C. (2013). Synthesis of mesoporous magnetic Co-NPs/carbon nanocomposites and their adsorption property for methyl orange from aqueous solution. *Journal of Colloid and Interface Science*, *389*(1), 10–15.

Zhu, H. Y., Jiang, R., Xiao, L., & Zeng, G. M. (2010). Preparation, characterization, adsorption kinetics and thermodynamics of novel magnetic chitosan enwrapping nanosized gamma-Fe2O3 and multi-walled carbon nanotubes with enhanced adsorption properties for methyl orange. *Bioresource Technology*, *101*(14), 5063–5069.